Improved electrochemical performance of $LiCoPO_4$ using eco-friendly aqueous binders

Eun Jeong Kim,[1,2] Xiangling Yue,[1] John T. S. Irvine,[1] and A. Robert Armstrong[1,2*]

[1] School of Chemistry, University of St Andrews, St Andrews, Fife KY16 9ST, United Kingdom

[2] ALISTORE-ERI, 80039, Amiens Cedex, France

[*]Corresponding author

Keywards

Lithium ion batteries, High-voltage positive electrode materials, Aqueous binders, $LiCoPO_4$

Abstract

The electrochemical performance of $LiCoPO_4$ (LCP) as a high-voltage positive electrode for lithium-ion batteries is significantly improved by using the aqueous binder sodium carboxymethyl cellulose (CMC). The CMC not only provides a uniform electrode surface as shown by scanning electron microscopy and elemental mapping, but also suppresses the degradation of $LiCoPO_4$ by scavenging HF in the electrolyte solution as demonstrated by FT-IR. In comparison with other water-soluble binders such as sodium alginate (ALG) and polyacrylic acid sodium salt (PAA), the homogeneous distribution of CMC within the electrodes accompanied by high accessibility of carboxylate groups in CMC are shown to be crucial factors to achieve enhanced performance with an excellent capacity retention of 94 % after 20 cycles at a rate of C/10.

Introduction

Lithium transition metal phosphates with the olivine structure have attracted much attention since the electrochemical activity of lithium iron phosphate (LFP) was first reported [1]. While LFP is already used in commercial lithium-ion batteries (LIB), there are growing studies on its counterparts with other transition metals. Among the phospho-olivine family, lithium cobalt phosphate (LCP) has been a strong candidate for high-voltage cathode materials since first identified by Amine et al, albeit with a limited initial discharge capacity of 70 $mAhg^{-1}$ [2]. However, the unsatisfactory electrochemical performance of LCP associated with low electronic [3-5] and ionic [6] conductivities as well as poor cycling stability [7-9] have been a major obstacle to its wide application. Extensive studies have been devoted to mitigating these limitations. Regarding the poor cycling performance of LCP, there are three main reasons: 1) the formation of undesired products on the surface of LCP [10-14], 2) the degradation of LCP by HF present in the electrolyte solution [15,16] and 3) the increase in the number of antisite cation exchange defects [17-19]. Most of the attempts to enhance the cyclability have included modifying LCP itself via doping [20-25] or surface modification [26-31] in combination with particle size reduction [22,32-34]. In addition to these strategies, the use of novel separators [35,36] and the development of functional electrolytes including additives [11,12,37] have been applied. In contrast, little attention has been paid to the inactive components such as conductive carbons and binders. These various approaches have improved cyclability with a peak performance of 153 $mAhg^{-1}$ observed in carbon coated nanosheets [32], though obtaining reliable high capacities remains a considerable challenge in this material.

Recently, the crucial role of binders in LIB performance has been highlighted [38]. In particular water-soluble binders have gained attention due to their enhanced interaction with active materials, stronger adhesion and mechanical buffer effect for volume change [39]. Considering these advantages, the introduction of aqueous binders in combination with LCP could be an important step for the development of high voltage positive electrode materials.

Here, we investigated the effect of three different aqueous binders (sodium carboxymethyl cellulose (CMC), sodium alginate (ALG) and polyacrylic acid sodium salt (PAA)) on the electrochemical

behaviour of LCP. These binders led to better electrochemical performance compared to polyvinylidene fluoride-based electrodes due to their excellent mechanical and chemical properties, acting as a protective agent for LCP. In addition, among these aqueous binders, CMC was found to significantly improve cycling stability and to suppress the degradation of LCP as confirmed by FT-IR analysis. The enhanced performance of LCP electrodes containing CMC demonstrates that the performance of pristine LCP can be improved simply by changing binder system, without any modification of LCP materials.

Experimental

Synthesis of $LiCoPO_4$ (LCP)

$LiCoPO_4$ (LCP) was synthesized by a solvothermal method previously reported by Brutti and co-workers [9,40] with slight modification. Two aqueous solutions: solution A with $LiOH{\cdot}H_2O$ (Sigma-Aldrich) and solution B containing LiH_2PO_4 (Alfa Aesar), $CoSO_4{\cdot}7H_2O$ (Sigma-Aldrich) and D-(+)-glucose (Sigma-Aldrich) were prepared separately. The solution A was added to ethylene glycol (EG) to give solution C. Subsequently the solution B was added dropwise into the solution C under stirring. The molar ratio of $LiOH{\cdot}H_2O$: $CoSO_4{\cdot}7H_2O$: LiH_2PO_4: D-(+)-glucose was 1.75:1:1:0.03. The Co^{2+} concentration in the final ethylene glycol/water solution was 0.1 M. The obtained purple suspension was sealed in a 135 ml Teflon-lined autoclave and heated in an oven at 220 °C for 16 h. The product was filtered, washed with water and ethanol then dried at 80 °C.

Characterisation

Powder X-ray diffraction patterns were recorded on a Stoe STADI/P diffractometer operating in transmission mode using Fe$K\alpha_1$ radiation (λ = 1.936 Å) in the 2θ range 20° – 80°. The samples were ground manually then supported between two clear polythene discs, held together by vacuum grease. During the measurement, the sample holder was spun to reduce preferred orientation effects. The structure was refined by the Rietveld method using the GSAS package with the EXPGUI interface [41]. Scanning electron microscopy (SEM) images of as-synthesized LCP material were recorded on a JEOL JSM-6700F instrument equipped with a field emission gun (FEG) electron source. Surface

morphology and elemental mapping of electrodes were obtained using an FEI Scios electron microscope equipped with EDAX Octane Plus EDS detector. ICP-OES analysis was performed using an iCAP 6000 Series. Fourier transform infrared (FT-IR) samples were prepared by mixing approximately 5 wt% of the material in dried KBr powder followed by pressing into a 10 mm diameter pellet. FT-IR spectra were recorded using a Nicolet Magna 860 spectrometer, with a deuterated-triglycine sulfate (DTGS) detector at a resolution of 4 cm^{-1}. 1024 scans were added together to achieve the desired signal to noise ratio. For ex-situ FT-IR measurements, electrodes were extracted from cycled cells and carefully rinsed with dried dimethyl carbonate (DMC) to remove residual electrolyte and then dried in a glovebox and a vacuum oven for 12 h.

Electrochemical characterisation

A slurry was prepared using the active material, super C65 carbon (IMERYS) and aqueous binders in the mass ratio 75:15:10, except where indicated. Binders used in this study were sodium carboxymethyl cellulose (CMC, degree of substitution (D.S.) = 1.2), sodium alginate (ALG), and polyacrylic acid sodium salt (PAA), all obtained from Sigma-Aldrich. The slurry was sonicated for 30 min then cast on aluminium foil by using a doctor blade. After drying at room temperature for 12 h, 12 mm diameter electrode discs were punched then dried at 130 °C under vacuum for 12 h. CR2325 coin cells (NRC, Canada) were assembled in an Ar-filled glovebox and used for evaluation of electrochemical performance. The cells consisted of a composite electrode, lithium foil as a counter/reference electrode (Sigma-Aldrich), a glass fibre separator (Whatman GF/F) and LP30 electrolyte (BASF, 1M $LiPF_6$ in ethylene carbonate (EC): dimethyl carbonate (DMC) = 1:1 w/w). The samples prepared are denoted as LCP-CMC, LCP-ALG and LCP-PAA for LCP electrodes fabricated with CMC, ALG and PAA binder, respectively. Additionally, LCP electrodes prepared with 5 wt% and 15 wt% CMC are denoted LCP-CMC-5 and LCP-CMC-15. An LCP-CMC (10 wt% of CMC) electrode, whose slurry was prepared by stirring rather than sonication is denoted LCP-CMC-S. Typical electrode loadings were 2.5 $mgcm^{-2}$, with a thickness of ca. 15 μm, irrespective of the binder used.

Half cells were tested by galvanostatic cycling at 30 °C in the potential window 3.5-5.0 V at C/10 based on a theoretical capacity of 167 $mAhg^{-1}$ using a Biologic Macpile II system. A series of five cycles at progressively increasing C-rates was carried out using a Maccor series 2200 system at 30 °C. Electrochemical impedance spectroscopy (EIS) measurements were conducted on coin cells. Data were collected using a Solartron 1255 frequency response analyser coupled with Solartron 1287 electrochemical interface. A perturbation voltage of 10 mV and frequency range from 0.1 Hz to 0.1 MHz were employed.

Results and discussion

LCP synthesis and characterisation

A powder X-ray diffraction (PXRD) pattern of the LCP material was recorded with Fe $K\alpha_1$ radiation (λ = 1.936 Å) to avoid Co fluorescence. A profile fit to the PXRD pattern is shown in Fig.1a. All diffraction peaks can be fully indexed on the basis of an orthorhombic olivine structure (space group *Pnma*, ICSD database no. 291401) with no additional peaks, indicating that single-phase LCP was obtained. The refined lattice parameters: a = 10.21806(10) Å, b = 5.92582(6) Å, c = 4.70650(5) Å are in good agreement with previously reported values [9,20,29,40,42,43]. Anti-site defects, involving the partial site exchange of Li and Co between 4a and 4c sites, affect the electrochemical performance by blocking Li^+ ion diffusion via 1D channels parallel to the [010] direction in the olivine structure. It is also known that the proportion of anti-site defects increases upon electrochemical cycling, leading to detrimental effects such as capacity fade and increased polarisation [17-19]. Refinement of the disorder revealed the presence of 3.5(1)% anti-site defects. Refinement considering a preferred orientation of the (0 1 0) plane resulted in an improved fit with R_{wP} 5.08 % implying that LCP particles are grown with exposed (010) faces, in keeping with the observed platelet morphology.

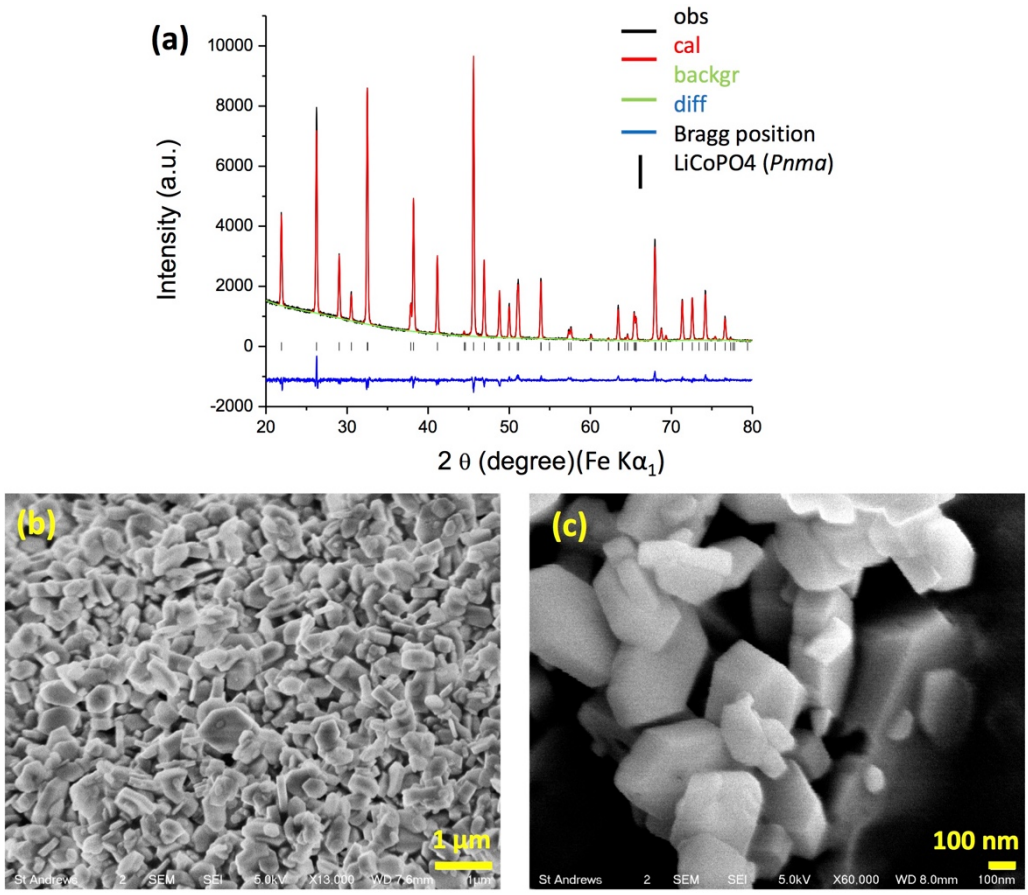

Figure 1. (a) Profile fit for powder XRD data from as-synthesized LCP. Observed data points are shown in black, with a fitted profile in red and the difference is shown in blue. Tick marks indicate allowed reflections. SEM images of LCP at (b) low- resolution and (c) high-resolution.

The low- and high-resolution SEM images of as-synthesized LCP are displayed in Fig. 1b-c. The LCP material consists of sub-micron hexagonal platelets, consistent with the reports that the ethylene glycol/water co-solvent system produces hexagonal platelets as well as reducing the particle size [43-45]. In the high-resolution SEM image (Fig.1c), the thickness of the LCP platelet-like particles is shown to be around 100-150 nm. Additional characterisation was carried out using FT-IR to confirm the successful synthesis of LCP material. In the FT-IR spectrum (Fig. S1), vibration features are analogous to those in the literature with stretching modes (1146, 1100, 1036, 977 cm^{-1}) and bending modes (636, 575, 550, 500, 473 cm^{-1}) [9,46].

Electrochemical performance of LCP electrodes prepared with different binders

Prior to performing electrochemical tests on LCP electrodes formulated using water-soluble binders, the stability of LCP in water was investigated. After soaking LCP in water for 6 h under stirring, no metal leaching nor degradation of LCP material was observed using ICP-OES, PXRD, and FT-IR (Fig.

S2), confirming the feasibility of employing aqueous binders to fabricate LCP electrodes. Subsequently, different LCP electrodes were prepared using the aqueous binders CMC, ALG and PAA. All these electrodes were formulated with the same amount of Super C65 carbon (15 wt%) and binder (10 wt%), then tested in coin cells.

Major differences in the electrochemical behaviour of CMC, ALG and PAA electrodes are evident after 20 cycles at C/10 (Fig. 2). The remarkable cyclability of the LCP-CMC electrode is clearly shown by the highest capacity retention of 94 %, followed by 72 % and 56 % for LCP-ALG and LCP-PAA, respectively. The initial capacity increase indicates that the LCP-CMC electrode requires some conditioning cycles to stabilize capacity [47,48].

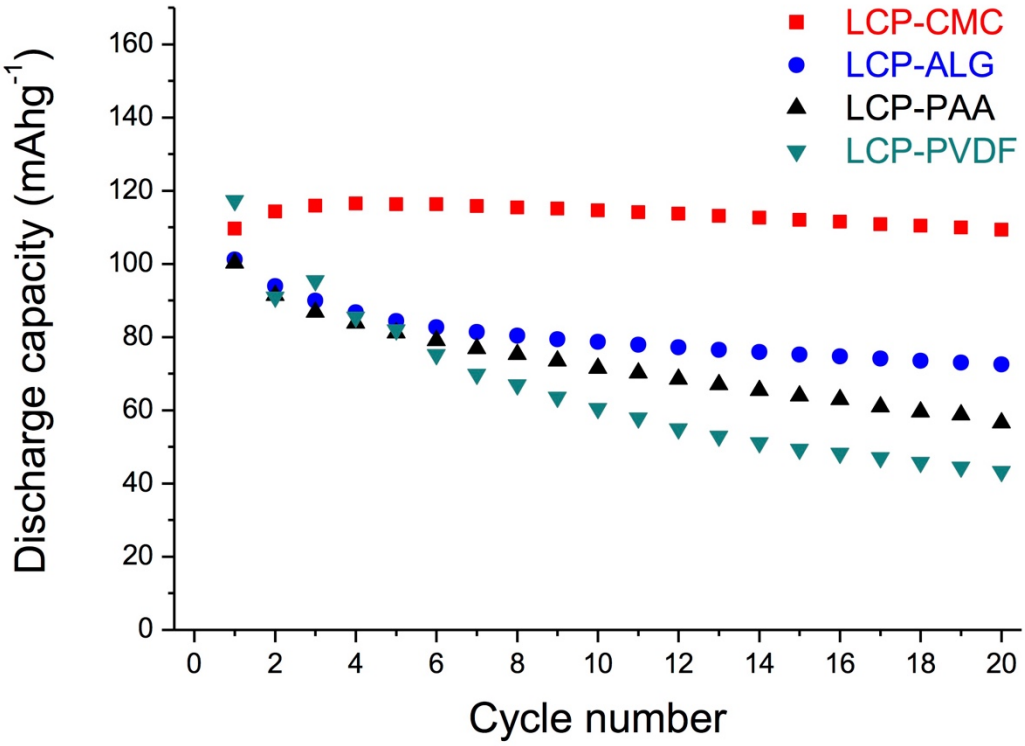

Figure 2. Galvanostatic cycling performance of LCP-CMC, LCP-ALG, LCP-PAA, and LCP-PVDF electrodes cycled at 30 °C between 3.5 and 5.0 V vs Li/Li$^+$ at a rate of C/10 (1C = 167 mAg^{-1})

Fig. 3 shows the charge/discharge curves of electrodes prepared with different water-soluble binders (CMC, ALG and PAA) at cycle 1, cycle 5 and cycle 20. It is known that the delithiation of LCP occurs in two stages, as indicated in schemes i and ii, with an intermediate phase of composition $Li_{2/3}CoPO_4$, coexisting with the fully lithiated phase ($LiCoPO_4$) at higher Li content and with the fully delithiated phase ($CoPO_4$) at low Li content upon charge [49-51].

i) $LiCoPO_4$ -> $Li_{2/3}CoPO_4$ + 1/3 Li^+ + 1/3 e^-

ii) $Li_{2/3}CoPO_4$ -> $CoPO_4$ + 2/3 Li^+ + 2/3 e^-

Both processes are reversible upon discharge, producing two plateaus in the voltage profiles (Fig. 3a-3c), and two oxidation peaks and two reduction peaks in dQ/dV curves (Fig. 3d). The charge/discharge plots of all electrodes at cycle 1 and cycle 5 show characteristic curves of LCP material with two distinct plateaus around 4.75 and 4.85 V. On the first cycle all electrodes show significant irreversible capacity with Coulombic efficiencies of 31 %, 24 % and 21 % for LCP-CMC, LCP-ALG and LCP-PAA respectively, due to electrolyte decomposition and possible solid-electrolyte interphase (SEI) layer formation at high voltage. It is noteworthy that the LCP-CMC electrode has the smallest polarisation from the initial cycle, maintaining this feature after 20 cycles. In order to gain a better understanding of the differences depending on binders after 20 cycles, the dQ/dV plots are shown in Fig. 3d. LCP-CMC displays the smallest differences in potential between oxidation and reduction peaks for the two processes, suggesting the fastest Li^+ insertion/extraction kinetics. In contrast, LCP-ALG exhibits slightly larger gaps with smaller magnitude especially in the first process ($LiCoPO_4$ -> $Li_{2/3}CoPO_4$ + 1/3 Li^+ + 1/3 e^-) probably due to some degradation of the LCP material. The degradation of LCP is clearly observed in the LCP-PAA electrode with the two peaks being barely distinguishable after 20 cycles.

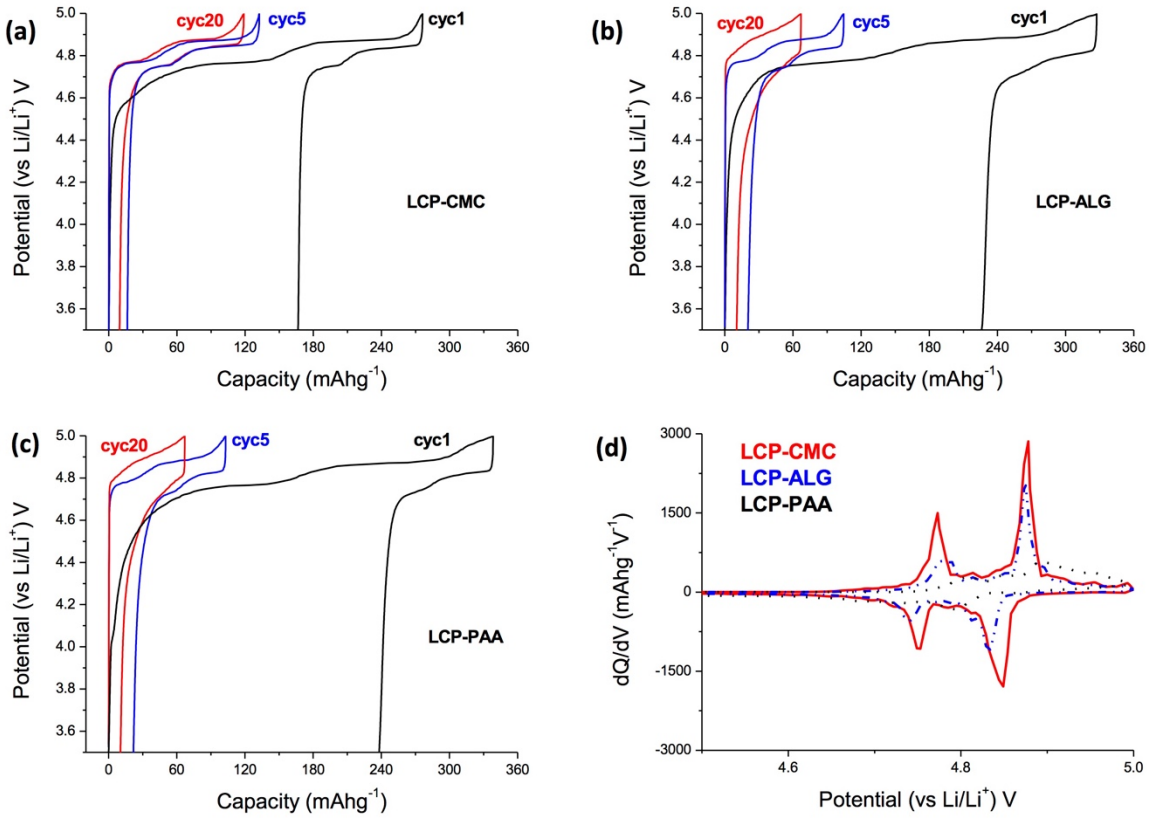

Figure 3. Charge/discharge curves at cycle 1, cycle 5 and cycle 20 for (a) LCP-CMC (b) LCP-ALG (c) LCP-PAA electrodes and (d) dQ/dV curves corresponding to cycle 20 of LCP-CMC (solid), LCP-ALG (dash) and LCP-PAA (dot) electrodes.

These results clearly show that the LCP-CMC electrode delivers the best capacity retention. Indeed, all aqueous binders exhibited better capacity retention than electrodes prepared using a conventional organic-soluble binder such as polyvinylidene fluoride (PVDF) which shows the highest polarisation on cycling leading to a capacity retention of 37 % over 20 cycles (Fig. 2 and Fig. S3).

In order to gain a better understanding of the different behaviour associated with the use of CMC, ALG and PAA, firstly the morphology of pristine electrodes was investigated. As shown in Fig. 4 and Fig. S4, the surface of the LCP-CMC electrode shows uniformly dispersed LCP without any cracks, whereas LCP-ALG and especially LCP-PAA electrodes have cracks on the surface and display aggregated LCP particles. All electrodes were further characterised by energy dispersive X-ray spectroscopy (EDS). The integral distribution of Co, P, O, C and Na elements in LCP-CMC electrode is presented in Fig. 4b. The Co, representing LCP particles (Fig. 4c), and Na, indicating CMC (Fig. 4d), are homogeneously distributed within the electrode. In contrast, LCP particles (Co) are aggregated in LCP-ALG (Fig. 4e-4h) and LCP-PAA electrodes (Fig. 4i-4l), which also show an

inhomogeneous binder distribution. This suggests that the nature of binder influences the morphology of the electrode, resulting in varying electrochemical performance; i.e. the percolating network between Super C65 carbon and LCP is hindered by the presence of cracks in the electrodes, leading to the increase in polarisation upon cycling. The morphology of the electrodes after 20 cycles was also investigated, confirming the robustness of LCP-CMC electrodes (Fig.S5).

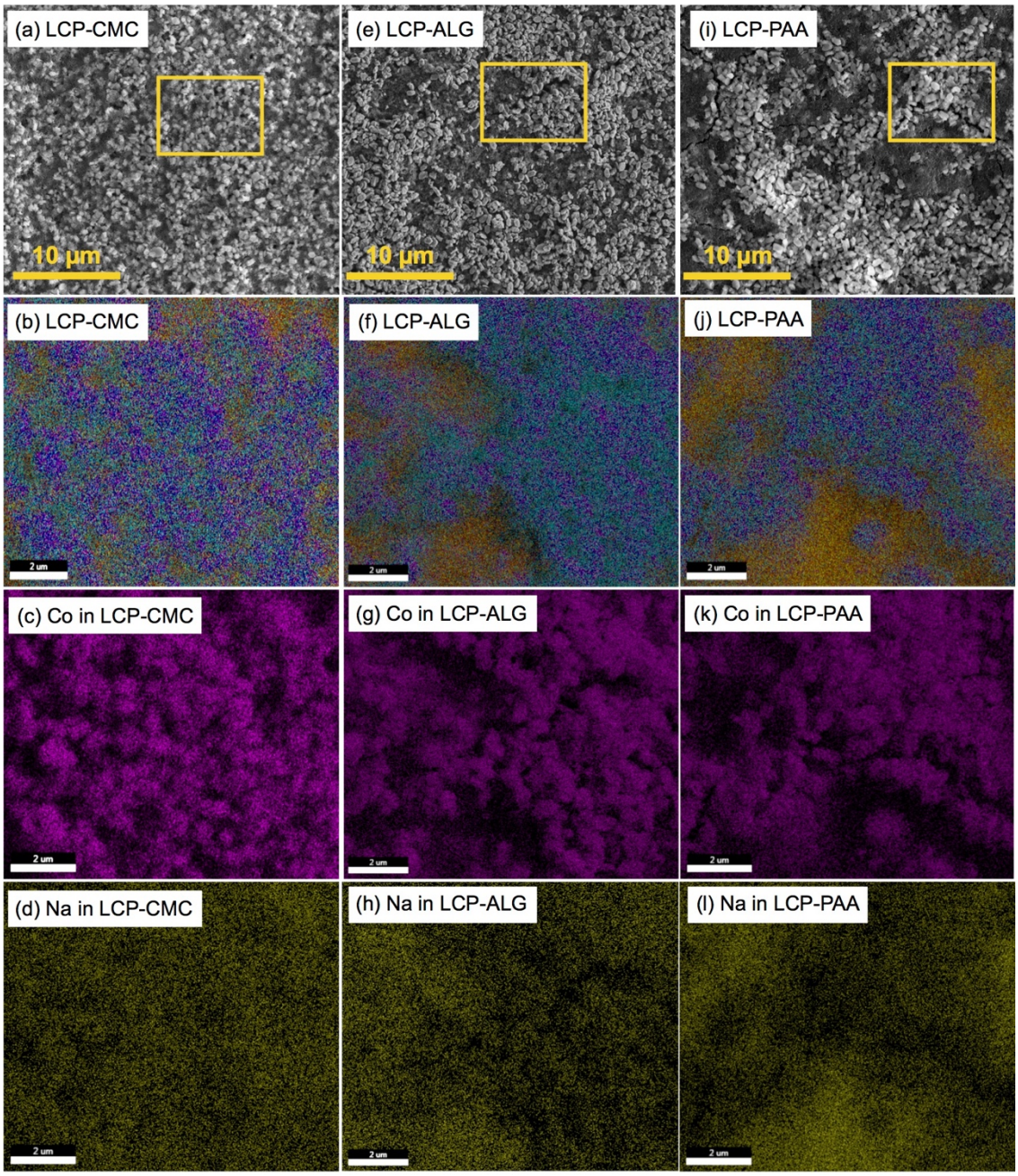

Figure 4. SEM image of (a) LCP-CMC, (e) LCP-ALG, (i) LCP-PAA electrode surfaces, EDS mapping (yellow frame) for (b,f,j) the integral distribution of Co (magenta), P (light blue), O (navy), C (orange) and Na (yellow), (c,g,k) Co distribution, (d,h,l) Na distribution in LCP-CMC, LCP-ALG and LCP-PAA electrode surfaces, respectively.

The significant cracks in the LCP-PAA electrode can be explained by examining the molecular structures of the binders (Fig. 5). CMC and ALG show a typical polysaccharide structure: glucose-like compounds containing 1.2 (CMC) to 1 (ALG) stoichiometric carboxylate groups, whereas PAA is a sodium salt of a homopolymer of acrylic acid with at least 3 times as many carboxylate groups as CMC or ALG. Thus, when dissolved in water, PAA will have a greater negative charge density on the surface, which could prevent a homogeneous distribution of binder with LCP particles that have a negative charge on the surface due to the PO_4^{3-} in neutral pH [52]. Another possible factor giving rise to the improved electrochemical performance of LCP-CMC electrodes lies in the mechanical properties of the binder, since CMC is the stiffest binder among those tested. From a chemical standpoint, polysaccharide-type binders such as CMC and ALG are less flexible than acrylic binders (PAA) due to the linear 1,4' β-glycosidic linkages between glucose-like monomers [53,54], which enables maintenance of the 3D network of Super C65 and LCP particles upon cycling. In the case of LCP-ALG, the presence of additional non-linear 1,4' α-glycosidic linkages may cause minor cracks in the electrode, resulting in moderate electrochemical performance compared to LCP-CMC.

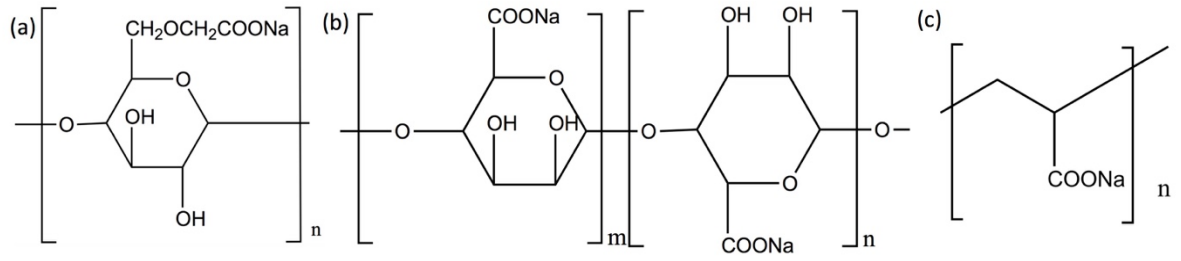

Figure 5. Molecular structure of binders (a) CMC, (b) ALG and (c) PAA.

In addition to the morphological effect, the carboxylate groups present in the aqueous binders studied in this work could improve the cycling stability. One of the reasons for the capacity fade of LCP-based materials is nucleophilic attack of F^- anions produced in $LiPF_6$ based electrolyte, resulting in the breakage of P-O bonds of the phosphate anions [15,16]. Indeed, HF is regenerated catalytically as a side product of the decomposition of LCP, causing a considerable capacity drop in the first few cycles. This detrimental phenomenon has been suppressed by HF scavenging. For example, improved capacity retention of LCP was obtained using quartz separators, as quartz can act as a sacrificial HF scavenger. In a study of $LiNi_{0.5}Mn_{1.5}O_4$, a carboxylate containing binder (PAA-Li) was used not only

as the binder but also as a passivating agent to suppress unstable electrode-electrolyte interfaces and undesirable side reactions by exchanging Li^+ ions in PAA-Li with protons from HF [55]. Therefore, it is reasonable to assume that the superior performance of aqueous binder based LCP electrodes over PVDF-based electrodes could originate from the presence of carboxylate groups that scavenge HF in the electrolyte. As seen in Fig. 5, the carboxylate groups in CMC are more accessible compared to those of ALG since CMC has an additional carbon atom between the cyclic backbone and the carboxylate groups. In addition, CMC contains 20 % more carboxylate groups than ALG due to the D.S. of 1.2. The unique structure of CMC combined with the higher carboxylate content could favour both HF-scavenging and Li^+ ion diffusion, resulting in improved performance.

Evidence for HF-scavenging was provided by FT-IR measurements. Fig. 6 displays FT-IR spectra for CMC binder, a freshly prepared LCP-CMC electrode and ex-situ LCP-CMC electrodes after 1 and 20 cycles. The FT-IR spectrum of the LCP-CMC electrode before cycling (Fig. 6b) shows spectral features of CMC and the LCP active material with a strong peak at 1612 cm^{-1}, characteristic of COONa in CMC. After 1 cycle (Fig. 6c), no significant change was observed except for the appearance of a peak at 807 cm^{-1}, corresponding to P-F stretching, which could be residual $LiPF_6$ salt or products of electrolyte decomposition [56]. After 20 cycles (Fig. 6d), additional peaks are observed at 1743 cm^{-1}, attributed to the carboxylic acid group (COOH) and at 1803 cm^{-1}, an anhydride -OCOOC-, resulting from the condensation reaction of two carboxylate groups and the loss of H_2O. The appearance of these two peaks supports the scavenging role of CMC through the following reaction: COONa + HF -> COOH + NaF. Moreover, the peak at 1612 cm^{-1} (COONa), which was observed for both the freshly prepared electrode and that after 1 cycle, shifts to a higher frequency of 1631 cm^{-1}. This peak can be assigned to COOLi [57] and provides direct evidence of Li^+ ion diffusion by a hopping mechanism via CMC, as previously observed in ALG based Si anodes [58].

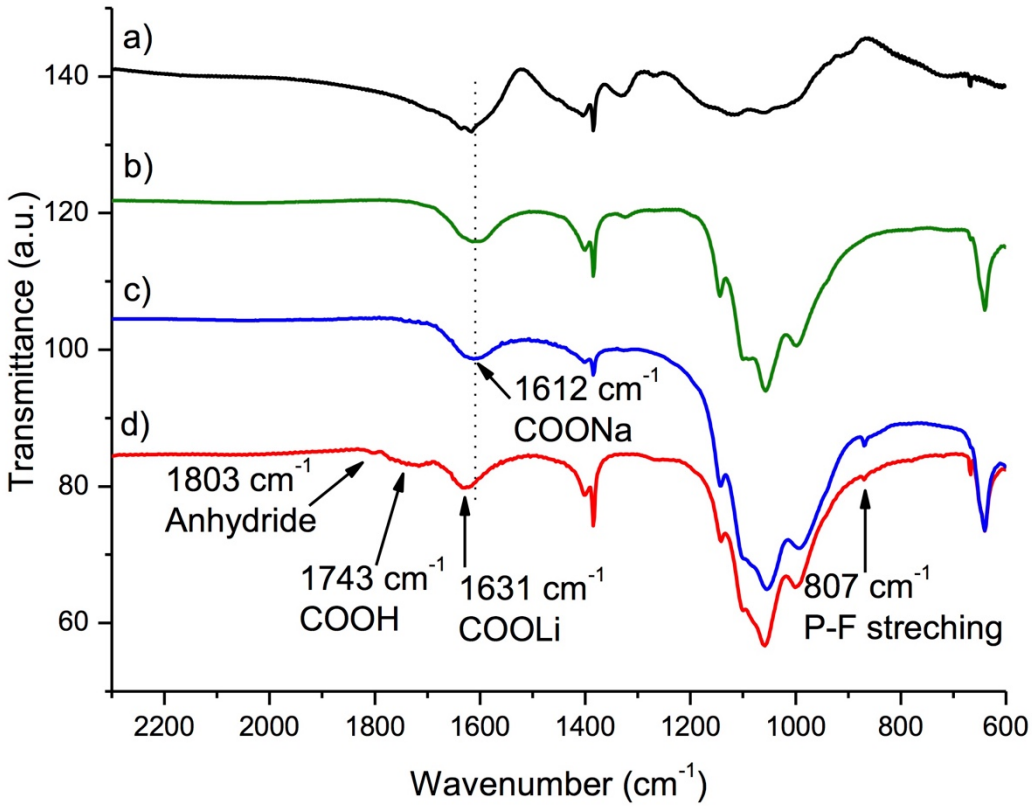

Figure 6. FT-IR of (a) CMC binder, (b) pristine LCP-CMC-15 electrode (c) LCP-CMC-15 after 1 cycle and (d) LCP-CMC-15 after 20 cycles.

To further support the hypothesis of HF-scavenging by CMC, we investigated 1) the effect of the quantity of CMC used and 2) the effect of slurry mixing method on electrochemical performance, considering that uniformly dispersed CMC could effectively cover the LCP by the formation of a protective interface between electrode and electrolyte, thus higher amounts of CMC could display better cycling performance.

As shown in Fig. 7, the capacity retention after 20 cycles of LCP-CMC-15 and LCP-CMC (10 wt% CMC) electrodes is excellent (93 % and 94 %, respectively), whereas LCP-CMC-5 exhibits 85 % capacity retention. Comparison of the charge/discharge profiles of LCP-CMC-15 and LCP-CMC-5 electrodes (Fig. 7b-c) demonstrates that the increase of polarisation after 20 cycles is less pronounced for LCP-CMC-15, implying that the higher amount of CMC provides a better protective interface between the LCP particles and electrolyte. However, the initial capacity tends to decrease as the amount of CMC increases. This can be attributed to slower Li^+ ion diffusion. Interestingly, despite an increase in the polarisation upon cycling for LCP-CMC-5, its energy efficiency is still better than

LCP-CMC and LCP-CMC-15 mainly due to better Coulombic efficiency (Fig. S6). However, as polarisation is reflected in the energy density [59], the energy density of LCP-CMC-5 decreases more significantly than its discharge capacity upon cycling compared to LCP-CMC-15. For LCP electrodes prepared using conventional mixing under stirring (LCP-CMC-S, 10 wt% CMC), only 72 % of the capacity was retained after 20 cycles. This lower performance of LCP-CMC-S implies a non-homogenous dispersion of the slurry components, which was confirmed by cross-section SEM images (Fig. S7). In the cross-section SEM image of an LCP-CMC electrode, a homogeneous network of Super C65 carbon and LCP particles is observed, whereas LCP-CMC-S has aggregated Super C65 with isolated active material. These results highlight that a homogeneous slurry dispersion is a crucial factor to fabricate a uniform electrode, which could also promote better coverage of CMC, leading to better electrochemical performance.

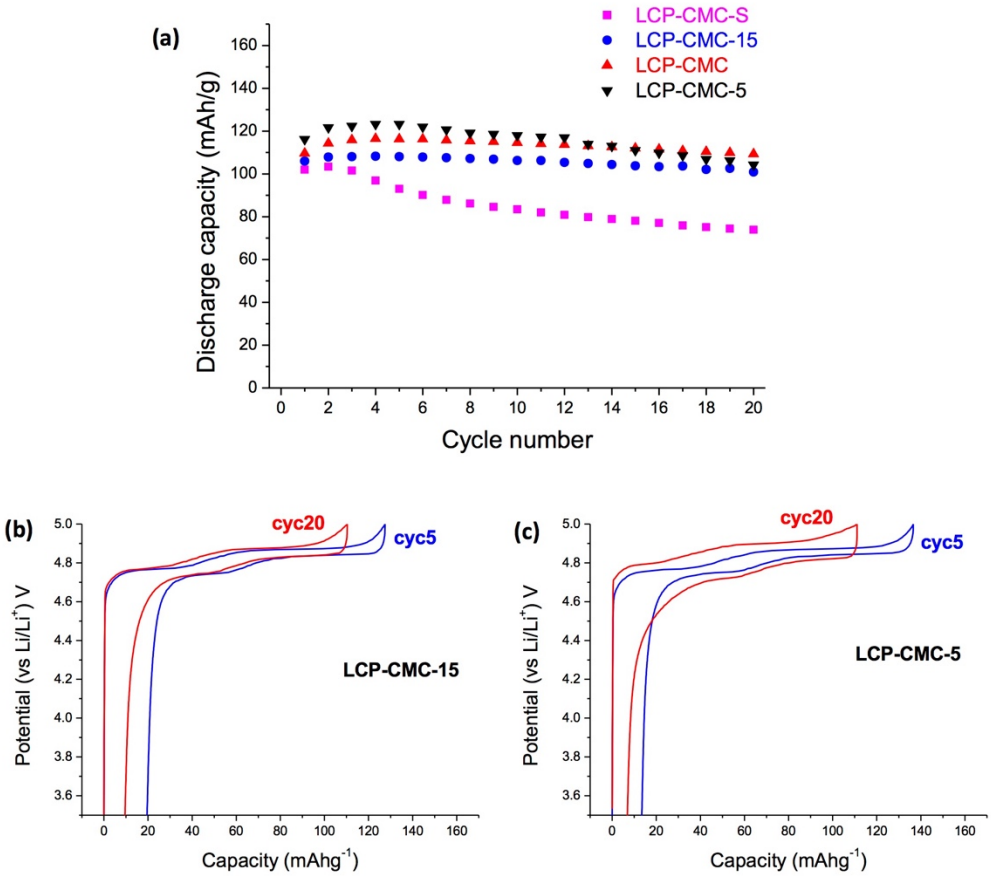

Figure 7. (a) Cycling performance of LCP electrodes, fabricated with different amounts of CMC and mixed in different ways, galvanostatically cycled at 30 °C in between 3.5 and 5.0 V vs Li/Li⁺ at a rate of C/10 (1C = 167 mAg⁻¹). Charge/discharge curves at cycle 5 and cycle 20 for (b) LCP-CMC-15 (c) LCP- CMC-5 electrodes.

The rate capability of electrodes made with each of the three binders was tested by galvanostatic cycling at different C-rates from C/10 to 2C (Fig. 8a). The results show that LCP-CMC exhibits significantly better rate performance overall, especially at 2C. In contrast, LCP-PAA demonstrates negligible capacity from C/2 to 2C, probably due to the lack of effective contact between LCP particles and conductive carbon as shown in SEM images (Fig.4i-l). It is noteworthy that LCP-CMC recovers its capacity at C/10, after cycling at higher rates, meaning that LCP materials were preserved without significant degradation.

Electrochemical impedance spectroscopy (EIS) measurements also confirmed the better performance of LCP-CMC electrodes. Fig. 8c shows the Nyquist plots of LCP-CMC, LCP-ALG and LCP-PAA electrodes after 20 cycles. LCP-CMC and LCP-ALG electrodes display an arc followed by an angled line whereas LCP-PAA exhibits an extra arc before the angled line. The size of the depressed arcs is the smallest in LCP-CMC followed by LCP-ALG and then LCP-PAA, in good agreement with electrochemical performance. Fitting results using an equivalent circuit (Table 1) reveal that analogous processes occur in LCP-CMC and LCP-ALG electrodes with resistances of 56.4 Ω and 116 Ω, respectively, due to an electrode process including LCP/electrolyte interface, SEI resistance and charge transfer within the electrodes as well as LCP particles. It is noted that R2 was included to fit LCP-PAA electrode but not in LCP-CMC and LCP-ALG electrodes, due to the appearance of an additional low frequency arc for the LCP-PAA electrode which represents a different process from that observed in other electrodes. Comparing the impedance results of electrodes after 20 cycles confirms that LCP-CMC shows the lowest resistance consistent with the smallest polarisation shift as shown in Fig. 3a.

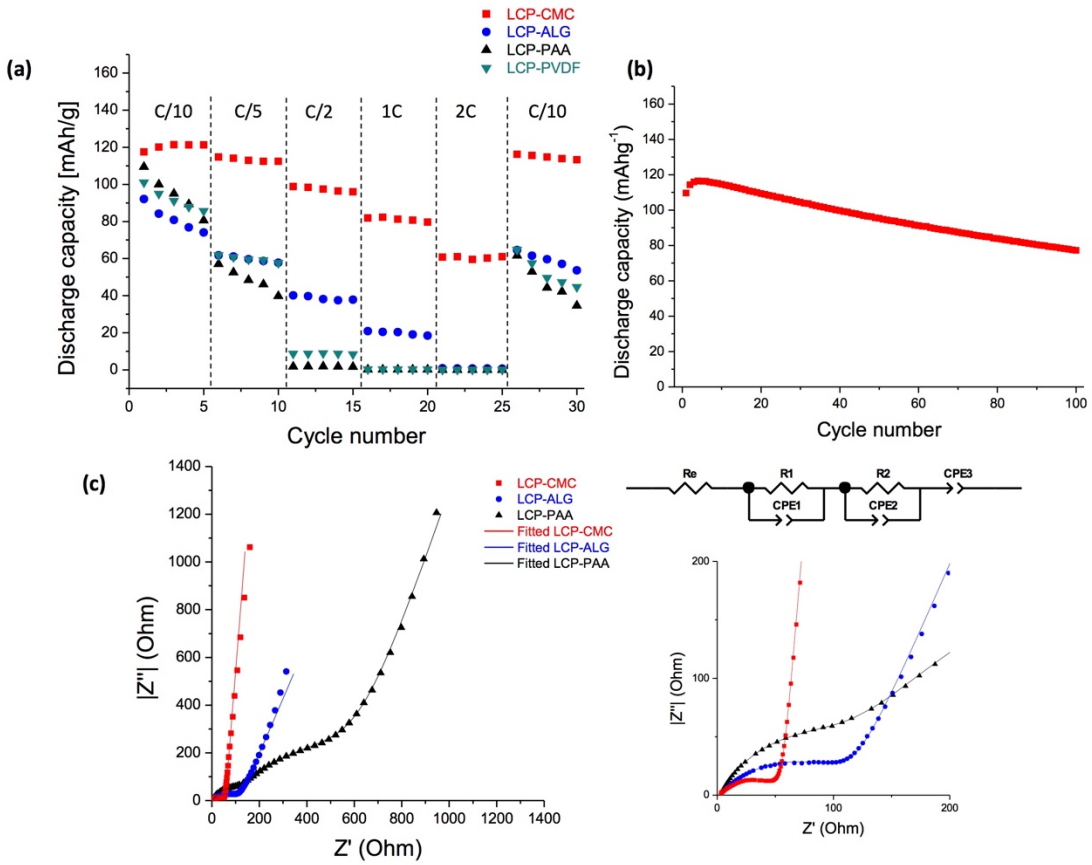

Figure 8. (a) Discharge capacity vs C-rate of LCP-CMC, LCP-ALG, LCP-PAA and LCP-PVDF electrodes. (b) Long term cycling performance of LCP-CMC galvanostatically cycled at 30 °C in between 3.5 and 5.0 V vs Li/Li⁺ at a rate of C/10 (1C = 167 mAg^{-1}) (c) Nyquist plots of LCP-CMC, LCP-ALG and LCP-PAA electrodes at frequencies from 0.1 Hz to 0.1MHz, with a zoomed image for high frequency and an equivalent circuit on the right.

	LCP-CMC	LCP-ALG	LCP-PAA
χ^2	4.15 x 10^{-4}	4.27 x 10^{-4}	1.10 x 10^{-4}
Re	1.56	2.46	2.65
R1	56.4	116	107
CPE1-T	3.2 x 10^{-4}	1.72 x 10^{-4}	2.47 x 10^{-5}
CPE1-P	0.523	0.544	0.733
R2	-	-	492
CPE2-T	-	-	2.35 x 10^{-4}
CPE2-P	-	-	0.677
CPE3-T	4.19 x 10^{-3}	2.45 x 10^{-3}	1.18 x 10^{-3}
CPE3-P	0.950	0.742	0.797

Table 1. Results of EIS fitting for LCP-CMC, LCP-ALG and LCP-PAA electrodes after 20 cycles using ZView2 applying an equivalent circuit.

Finally, the long-term cycling stability of LCP-CMC was investigated at a rate of C/10 (Fig. 8b), indicating that this composite shows good capacity retention of 68 % after 100 cycles, which compares favourably with previously reported studies. It is also important to note that this electrode was prepared without any special treatments and was cycled at C/10 where LCP particles are more exposed to electrolyte while other studies reported improved capacity retention through carbon coating or morphology control of LCP with 62 % at C/5 [35] and 68 % at C/2 [44], respectively.

Conclusion

In summary, we have tested CMC, ALG and PAA as aqueous binders for LCP electrodes. The influence of structure and functional group of the binders on the electrochemical performances of LCP electrodes was investigated, demonstrating that the stiffness and the presence of carboxylate groups are essential to prevent LCP particles from HF attack. With good stiffness and highly accessible carboxylate groups, CMC showed excellent ability as both binder and HF scavenger, compared to other binders.

Acknowledgements

EJK would like to thank the Alistore ERI for the award of a studentship. The authors thank EPSRC Capital for Great Technologies Grant EP/L017008/1.

References

[1] A.K. Padhi, K.S. Nanjundaswamy, J.B. Goodenough, Phospho- olivines as Positive- Electrode Materials for Rechargeable Lithium Batteries, Journal of the Electrochemical Society. 144 (1997) 1188–1194. doi:10.1149/1.1837571.

[2] K. Amine, H. Yasuda, M. Yamachi, Olivine LiCoPO4 as 4.8 V Electrode Material for Lithium Batteries, Electrochem. Solid-State Lett. 3 (2000) 178–179. doi:10.1149/1.1390994.

[3] Electrical conductivity of doped LiCoPO4, Journal of Power Sources. 158 (2006) 1431–1435. doi:10.1016/j.jpowsour.2005.10.072.

[4] J.L. Allen, T. Thompson, J. Sakamoto, C.R. Becker, T.R. Jow, J. Wolfenstine, Transport properties of LiCoPO4 and Fe-substituted LiCoPO4, Journal of Power Sources. 254 (2014) 204–208. doi:10.1016/j.jpowsour.2013.12.111.

[5] M.E. Rabanal, M.C. Gutierrez, F. Garcia-Alvarado, E.C. Gonzalo, M.E. Arroyo-de Dompablo, Improved electrode characteristics of olivine–LiCoPO4 processed by high energy milling, Journal of Power Sources. 160 (2006) 523–528. doi:10.1016/j.jpowsour.2005.12.071.

[6] M. Prabu, S. Selvasekarapandian, A.R. Kulkarni, S. Karthikeyan, G. Hirankumar, C. Sanjeeviraja, Ionic transport properties of LiCoPO4 cathode material, Solid State Sciences. 13 (2011) 1714–1718. doi:10.1016/j.solidstatesciences.2011.06.023.

[7] N.N. Bramnik, K.G. Bramnik, T. Buhrmester, C. Baehtz, H. Ehrenberg, H. Fuess, Electrochemical and structural study of LiCoPO4-based electrodes, J Solid State Electrochem. 8 (2004) 558–564. doi:10.1007/s10008-004-0497-x.

[8] B. Jin, H.-B. Gu, K.-W. Kim, Effect of different conductive additives on charge/discharge properties of LiCoPO4/Li batteries, J Solid State Electrochem. 12 (2007) 105–111. doi:10.1007/s10008-007-0367-4.

[9] S. Brutti, J. Manzi, A. De Bonis, D. Di Lecce, F. Vitucci, A. Paolone, et al., Controlled synthesis of LiCoPO4 by a solvo-thermal method at 220°C, Materials Letters. 145 (2015) 324–327. doi:10.1016/j.matlet.2015.01.137.

[10] N.N. Bramnik, K. Nikolowski, C. Baehtz, K.G. Bramnik, H. Ehrenberg, Phase Transitions Occurring upon Lithium Insertion–Extraction of LiCoPO 4, Chem. Mater. 19 (2007) 908–915. doi:10.1021/cm062246u.

[11] R. Sharabi, E. Markevich, K. Fridman, G. Gershinsky, G. Gershinsky, G. Salitra, et al., Electrolyte solution for the improved cycling performance of LiCoPO4/C composite cathodes, Electrochemistry Communications. 28 (2013) 20–23. doi:10.1016/j.elecom.2012.12.001.

[12] L.Y. Xing, M. Hu, Q. Tang, J.P. Wei, X. Qin, Z. Zhou, Improved cyclic performances of LiCoPO4/C cathode materials for high-cell-potential lithium-ion batteries with thiophene as an electrolyte additive, Electrochimica Acta. 59 (2012) 172–178. doi:10.1016/j.electacta.2011.10.054.

[13] E. Markevich, G. Salitra, K. Fridman, R. Sharabi, G. Gershinsky, A. Garsuch, et al., Fluoroethylene Carbonate as

an Important Component in Electrolyte Solutions for High-Voltage Lithium Batteries: Role of Surface Chemistry on the Cathode, Langmuir. 30 (2014) 7414–7424. doi:10.1021/la501368y.

[14] J. Manzi, S. Brutti, Surface chemistry on LiCoPO 4 electrodes in lithium cells: SEI formation and self-discharge, Electrochimica Acta. 222 (2016) 1839–1846. doi:10.1016/j.electacta.2016.11.175.

[15] R. Sharabi, E. Markevich, V. Borgel, G. Salitra, G. Gershinsky, D. Aurbach, et al., Raman study of structural stability of LiCoPO4 cathodes in LiPF6 containing electrolytes, Journal of Power Sources. 203 (2012) 109–114. doi:10.1016/j.jpowsour.2011.12.018.

[16] E. Markevich, R. Sharabi, H. Gottlieb, V. Borgel, K. Fridman, G. Salitra, et al., Reasons for capacity fading of LiCoPO4 cathodes in LiPF6 containing electrolyte solutions, Electrochemistry Communications. 15 (2012) 22–25. doi:10.1016/j.elecom.2011.11.014.

[17] Q.D. Truong, M.K. Devaraju, Y. Sasaki, H. Hyodo, T. Tomai, I. Honma, Relocation of Cobalt Ions in Electrochemically Delithiated LiCoPO4Cathode Materials, Chem. Mater. 26 (2014) 2770–2773. doi:10.1021/cm501452p.

[18] A. Boulineau, T. Gutel, Revealing Electrochemically Induced Antisite Defects in LiCoPO4: Evolution upon Cycling, Chem. Mater. 27 (2015) 802–807. doi:10.1021/cm503716p.

[19] Y.H. Ikuhara, X. Gao, C.A.J. Fisher, A. Kuwabara, H. Moriwake, K. Kohama, et al., Atomic level changes during capacity fade in highly oriented thin films of cathode material LiCoPO4, J. Mater. Chem. A. 5 (2017) 9329–9338. doi:10.1039/C6TA10084H.

[20] D. Di Lecce, J. Manzi, F.M. Vitucci, A. De Bonis, S. Panero, S. Brutti, Effect of the iron doping in LiCoPO4 cathode materials for lithium cells, Electrochimica Acta. 185 (2015) 17–27. doi:10.1016/j.electacta.2015.10.107.

[21] N.V. Kosova, O.A. Podgornova, E.T. Devyatkina, V.R. Podugolnikov, S.A. Petrov, Effect of Fe 2+substitution on the structure and electrochemistry of LiCoPO 4prepared by mechanochemically assisted carbothermal reduction, Journal of Materials Chemistry a: Materials for Energy and Sustainability. 2 (2014) 20697–20705. doi:10.1039/C4TA04221B.

[22] L. Fang, H. Zhang, Y. Zhang, L. Liu, Y. Wang, Design and synthesis of two-dimensional porous Fe-doped LiCoPO4 nano-plates as improved cathode for lithium ion batteries, Journal of Power Sources. 312 (2016) 101–108. doi:10.1016/j.jpowsour.2016.02.035.

[23] H. Li, Y. Wang, X. Yang, L. Liu, L. Chen, J. Wei, Improved electrochemical performance of 5 V LiCoPO 4 cathode materials via yttrium doping, Solid State Ionics. 255 (2014) 84–88. doi:10.1016/j.ssi.2013.12.007.

[24] J.L. Allen, T.R. Jow, J. Wolfenstine, Improved cycle life of Fe-substituted LiCoPO4, Journal of Power Sources. 196 (2011) 8656–8661. doi:10.1016/j.jpowsour.2011.06.057.

[25] F. Wang, J. Yang, Y. NuLi, J. Wang, Highly promoted electrochemical performance of 5V LiCoPO4 cathode material by addition of vanadium, Journal of Power Sources. 195 (2010) 6884–6887. doi:10.1016/j.jpowsour.2010.04.071.

[26] A. Örnek, An impressive approach to solving the ongoing stability problems of LiCoPO4 cathode: Nickel oxide surface modification with excellent core-shell principle, Journal of Power Sources. 356 (2017) 1–11. doi:10.1016/j.jpowsour.2017.04.074.

[27] Y. Maeyoshi, S. Miyamoto, Y. Noda, H. Munakata, K. Kanamura, Effect of organic additives on characteristics of carbon-coated LiCoPO4 synthesized by hydrothermal method, Journal of Power Sources. 337 (2017) 92–99. doi:10.1016/j.jpowsour.2016.10.106.

[28] A. Örnek, M. Can, A. Yeşildağ, Improving the cycle stability of LiCoPO4 nanocomposites as 4.8V cathode: Stepwise or synchronous surface coating and Mn substitution, Materials Characterization. 116 (2016) 76–83. doi:10.1016/j.matchar.2016.04.009.

[29] B. Wu, H. Xu, D. Mu, L. Shi, B. Jiang, L. Gai, et al., Controlled solvothermal synthesis and electrochemical performance of LiCoPO4 submicron single crystals as a cathode material for lithium ion batteries, Journal of Power Sources. 304 (2016) 181–188. doi:10.1016/j.jpowsour.2015.11.023.

[30] N. Laszczynski, A. Birrozzi, K. Maranski, M. Copley, M.E. Schuster, S. Passerini, Effect of coatings on the green electrode processing and cycling behaviour of LiCoPO 4, Journal of Materials Chemistry a: Materials for Energy and Sustainability. 4 (2016) 17121–17128. doi:10.1039/C6TA05262B.

[31] J. Ni, L. Gao, L. Lu, Carbon coated lithium cobalt phosphate for Li-ion batteries: Comparison of three coating techniques, Journal of Power Sources. 221 (2013) 35–41. doi:10.1016/j.jpowsour.2012.07.107.

[32] X. Rui, X. Zhao, Z. Lu, H. Tan, D. Sim, H.H. Hng, et al., Olivine-Type Nanosheets for Lithium Ion Battery Cathodes, ACS Nano. 7 (2013) 5637–5646. doi:10.1021/nn4022263.

[33] M.K. Devaraju, D. Rangappa, I. Honma, Controlled synthesis of plate-like LiCoPO4 nanoparticles via supercritical method and their electrode property, Electrochimica Acta. 85 (2012) 548–553. doi:10.1016/j.electacta.2012.08.108.

[34] J. Liu, T.E. Conry, X. Song, L. Yang, M.M. Doeff, T.J. Richardson, Spherical nanoporous LiCoPO4/C composites as high performance cathode materials for rechargeable lithium-ion batteries, Journal of Materials Chemistry. 21 (2011) 9984–9987. doi:10.1039/C1JM10793C.

[35] R. Sharabi, E. Markevich, V. Borgel, G. Salitra, D. Aurbach, G. Semrau, et al., Significantly improved cycling performance of LiCoPO4 cathodes, Electrochemistry Communications. 13 (2011) 800–802. doi:10.1016/j.elecom.2011.05.006.

[36] Y. Maeyoshi, S. Miyamoto, H. Munakata, K. Kanamura, Enhanced cycle stability of LiCoPO4 by using three-dimensionally ordered macroporous polyimide separator, Journal of Power Sources. 350 (2017) 103–108. doi:10.1016/j.jpowsour.2017.03.053.

[37] T. Fukutsuka, T. Nakagawa, K. Miyazaki, T. Abe, Electrochemical properties of LiCoPO 4 -thin film electrodes in LiF-based electrolyte solution with anion receptors, Journal of Power Sources. 306 (2016) 753–757. doi:10.1016/j.jpowsour.2015.12.105.

[38] S.-L. Chou, Y. Pan, J.-Z. Wang, H.-K. Liu, S.-X. Dou, Small things make a big difference: binder effects on the performance of Li and Na batteries, Phys. Chem. Chem. Phys. 16 (2014) 20347–20359. doi:10.1039/C4CP02475C.

[39] J.-T. Li, Z.-Y. Wu, Y.-Q. Lu, Y. Zhou, Q.-S. Huang, L. Huang, et al., Water Soluble Binder, an Electrochemical Performance Booster for Electrode Materials with High Energy Density, Advanced Energy Materials. 451 (2017) 1701185–30. doi:10.1002/aenm.201701185.

[40] J. Manzi, M. Curcio, S. Brutti, Structural and Morphological Tuning of LiCoPO4 Materials Synthesized by Solvo-Thermal Methods for Li-Cell Applications, Nanomaterials. 5 (2015) 2212–2230. doi:10.3390/nano5042212.

[41] B.H. Toby, EXPGUI, a graphical user interface for GSAS.

[42] J. Manzi, F.M. Vitucci, A. Paolone, F. Trequattrini, S. Panero, D. Di Lecce, et al., Analysis of the self-discharge process in LiCoPO4 electrodes: bulks, Electrochimica Acta. 179 (2015) 604–610. doi:10.1016/j.electacta.2015.03.071.

[43] J. Ludwig, C. Marino, D. Haering, C. Stinner, H.A. Gasteiger, T. Nilges, Morphology-controlled microwave-assisted solvothermal synthesis of high-performance LiCoPO 4 as a high-voltage cathode material for Li-ion batteries, Journal of Power Sources. 342 (2017) 214–223. doi:10.1016/j.jpowsour.2016.12.059.

[44] J. Ludwig, J. Ludwig, C. Marino, C. Marino, D. Haering, C. Stinner, et al., Facile, ethylene glycol-promoted microwave-assisted solvothermal synthesis of high-performance LiCoPO4 as a high-voltage cathode material for lithium-ion batteries, RSC Adv. 6 (2016) 82984–82994. doi:10.1039/C6RA19767A.

[45] X. Qin, X. Wang, H. Xiang, J. Xie, J. Li, Y. Zhou, Mechanism for Hydrothermal Synthesis of LiFePO4Platelets as Cathode Material for Lithium-Ion Batteries, The Journal of Physical Chemistry C. 114 (2010) 16806–16812. doi:10.1021/jp104466e.

[46] A.A. Salah, P. Jozwiak, K. Zaghib, J. Garbarczyk, F. Gendron, A. Mauger, et al., FTIR features of lithium-iron phosphates as electrode materials for rechargeable lithium batteries, Spectrochimica Acta Part a: Molecular and Biomolecular Spectroscopy. 65 (2006) 1007–1013. doi:10.1016/j.saa.2006.01.019.

[47] F. De Giorgio, N. Laszczynski, J. von Zamory, M. Mastragostino, C. Arbizzani, S. Passerini, Graphite//LiNi0.5Mn1.5O4 Cells Based on Environmentally Friendly Made- in- Water Electrodes, ChemSusChem. 10 (2017) 379–386. doi:10.1002/cssc.201601249.

[48] W.-Y. Chou, Y.-C. Jin, J.-G. Duh, C.-Z. Lu, S.-C. Liao, A facile approach to derive binder protective film on high voltage spinel cathode materials against high temperature degradation, Applied Surface Science. 355 (2015) 1272–1278. doi:10.1016/j.apsusc.2015.08.046.

[49] M.G. Palmer, J.T. Frith, A.L. Hector, A.W. Lodge, J.R. Owen, C. Nicklin, et al., In situ phase behaviour of a high capacity LiCoPO4 electrode during constant or pulsed charge of a lithium cell, Chemical Communications. 52 (2016) 14169–14172. doi:10.1039/C6CC07756K.

[50] F.C. Strobridge, R.J. Clément, M. Leskes, D.S. Middlemiss, O.J. Borkiewicz, K.M. Wiaderek, et al., Identifying the Structure of the Intermediate, Li 2/3CoPO 4, Formed during Electrochemical Cycling of LiCoPO 4, Chem. Mater. 26 (2014) 6193–6205. doi:10.1021/cm502680w.

[51] M. Kaus, I. Issac, R. Heinzmann, S. Doyle, S. Mangold, H. Hahn, et al., Electrochemical Delithiation/Relithiation of LiCoPO 4: A Two-Step Reaction Mechanism Investigated by in SituX-ray Diffraction, in SituX-ray Absorption Spectroscopy, and ex Situ7Li/ 31P NMR Spectroscopy, The Journal of Physical Chemistry C. 118 (2014) 17279–17290. doi:10.1021/jp503306v.

[52] J. Li, B.L. Armstrong, J. Kiggans, C. Daniel, D.L. Wood III, Optimization of LiFePO 4Nanoparticle Suspensions with Polyethyleneimine for Aqueous Processing, Langmuir. 28 (2012) 3783–3790. doi:10.1021/la205157d.

[53] F. Jeschull, F. Lindgren, M.J. Lacey, F.B. refors, K.E. m, D. Brandell, Influence of inactive electrode components on degradation phenomena in nano-Si electrodes for Li-ion batteries, Journal of Power Sources. 325 (2016) 513–524. doi:10.1016/j.jpowsour.2016.06.059.

[54] C. Hwang, S. Joo, N.-R. Kang, U. Lee, T.-H. Kim, Y. Jeon, et al., Breathing silicon anodes for durable high-power operations, Scientific Reports. 5 (2015) srep14433. doi:10.1038/srep14433.

[55] N.P.W. Pieczonka, V. Borgel, B. Ziv, N. Leifer, V. Dargel, D. Aurbach, et al., Lithium Polyacrylate (LiPAA) as an Advanced Binder and a Passivating Agent for High- Voltage Li- Ion Batteries, Advanced Energy Materials. 5 (2015) 1501008. doi:10.1002/aenm.201501008.

[56] C. Schultz, S. Vedder, B. Streipert, M. Winter, S. Nowak, Quantitative investigation of the decomposition of organic lithium ion battery electrolytes with LC-MS/MS, RSC Adv. 7 (2017) 27853–27862. doi:10.1039/C7RA03839A.

[57] F.M. Courtel, S. Niketic, D. Duguay, Y. Abu-Lebdeh, I.J. Davidson, Water-soluble binders for MCMB carbon anodes for lithium-ion batteries, Journal of Power Sources. 196 (2011) 2128–2134. doi:10.1016/j.jpowsour.2010.10.025.

[58] I. Kovalenko, B. Zdyrko, A. Magasinski, B. Hertzberg, Z. Milicev, R. Burtovyy, et al., A Major Constituent of Brown Algae for Use in High-Capacity Li-Ion Batteries, Science. 334 (2011) 75–79. doi:10.1126/science.1209150.

[59] A. Eftekhari, Energy efficiency: a critically important but neglected factor in battery research, Sustainable Energy Fuels, 2017, 1, 2053. doi: 10.1039/c7se00350a